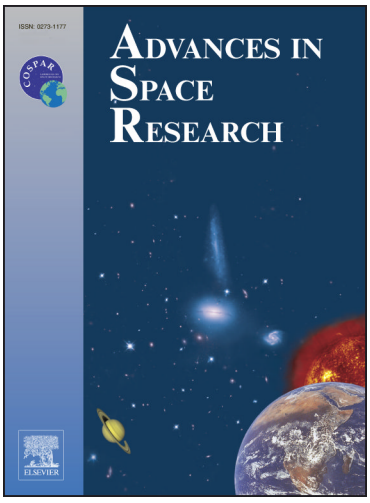

Grid fins shape design of a launch vehicle based on sequential approximation optimization

Ke Peng, Fan Hu, Donghui Wang, Patrick N Okolo, Min Xiang, Gareth J. Bennett, Weihua Zhang

PII: S0273-1177(18)30467-8
DOI: https://doi.org/10.1016/j.asr.2018.06.001
Reference: JASR 13783

To appear in: *Advances in Space Research*

Received Date: 19 April 2018
Revised Date: 1 June 2018
Accepted Date: 2 June 2018

Please cite this article as: Peng, K., Hu, F., Wang, D., Okolo, P.N., Xiang, M., Bennett, G.J., Zhang, W., Grid fins shape design of a launch vehicle based on sequential approximation optimization, *Advances in Space Research* (2018), doi: https://doi.org/10.1016/j.asr.2018.06.001

Grid fins shape design of a launch vehicle based on sequential approximation optimization

Ke Peng[1], Fan Hu[1], Donghui Wang[1*], Patrick N Okolo. N[2], Min Xiang[1], Gareth J. Bennett[2], Weihua Zhang[1]

(1. College of Aerospace Science and Engineering, National University of Defense Technology, Changsha, Hunan 410073, People's Republic of China;
2. Department of Mechanical and Manufacturing Engineering, University of Dublin, Trinity College, Dublin 2, Ireland)

Abstract: This paper performed the optimization of grid fins shape of a launch vehicle based on Sequential Approximation Optimization (SAO) and Computational Fluid Dynamics (CFD) simulation coupling. An efficient and reliable method is proposed for determining the width of Gaussian functions based on a logical relationship between the width and local density. The performance of the proposed method is evaluated using five classical test functions. The proposed method for width determination generates almost no excessive calculation costs, and improves the accuracy, reliability, and stability of the Radial Basis Function (RBF) surrogate model notably. Based on the improved RBF surrogate model, a framework and detailed procedure for the SAO algorithm is presented, and the performance of the proposed SAO algorithm is tested, with obtained results showing that the proposed SAO algorithm reduces the calling times of the original model and improves the optimization efficiency remarkably. The objective function is strictly deduced and reflects the momentum loss caused by aerodynamic drag directly. Three constraints are imposed to ensure the static stability and controllability of the launch vehicle. Finally, grid fins shape optimization problem of the launch vehicle is solved, with the objective function and constraints calculation tasks accomplished automatically by batch mode CFD simulations. The global optimal solution is obtained after 54 calling times of the original model, and 92 hours (3.84 days) of computation on a 96-core cluster. Once the baseline shape is replaced with the optimized shape, it is detected that (1) taking the minimum fuel as an objective function, the take-off mass is 2.07% lighter than the take-off mass of the baseline shape, (2) taking the maximum payload mass as an objective function, the payload mass is 14.3% heavier than the payload mass of the baseline shape.

Keywords: *Grid fins; Launch vehicle; Sequential approximation optimization; Radial basis function model; width of Gaussian functions; Shape optimization*

1 Introduction

Grid fins (also known as lattice fins) are non-conventional aerodynamic lifting and control surfaces which consists of outer frames and intersecting grids. The main advantages of grid fins includes; (1) favorable lift characteristics, (2) very high stall angle of attack, (3) low hinge moment due to low chord length, hence small size of needed control actuator, (4) can be easily folded for efficient packaging, storage, and transport, (5) high strength to mass ratio (Theerthamalai, 2007; Peng, 2015). Due to its advantages, grid fins have attracted much attention in recent years and have been utilized for a wide variety of missiles and intelligent munition systems successfully, examples which include; the OTR-21 Tochka tactical ballistic missile of the Former Soviet Union, R-77 air-to-air missile of Russia, GBU-43/B Massive Ordnance Air Blast (MOAB) of the USA, Falcon 9 rocket, Falcon heavy rocket, etc. Due to its favorable characteristics, grid fins can also be used as stabilizing and control surfaces of launch vehicles appropriately, an example of which the Chinese Kuaizhou 1 and Kuaizhou 11 launch vehicle possess four grid fins installed on the base of the first stage. However, the main disadvantages of grid fins are (1) Its complex shape and structure, (2) higher drag when compared with conventional fins.

Aerodynamic shape design of grid fins are highly essential and presents the major consideration during grid fin designs. A more careful and detailed aerodynamic shape design could further develop and improve the advantages of grid fins, and in so doing,

* Corresponding author
Email addresses: wangdonghui1984@sina.cn (D. Wang).

potentially reduce the impacts of its associated disadvantages. Existing studies mainly focused on; grid fins basic aerodynamic characteristics (Dikbas and Baran et al., 2018; Kless and Aftosmis, 2011; Hughson and Blades et al., 2007; Simpson and Sadler, 1998), effects of geometric variables on grid fins aerodynamic characteristics (Washington and Miller, 1998), special configurations such as curved grid fins (Washington and Booth et al., 1993), and local swept back grid fins (Guyot and Schulein, 2007), etc. Meanwhile, studies on grid fins aerodynamic shape design based on modern numerical optimization methods was seldomly found, except for studies by; Yang and Zhang (2013), where they optimized three section shape parameters of grid fins base on Computational Fluid Dynamics (CFD) method, and Ledlow and Burkhalter et al. (2015), whom optimized a ten grid fin geometrical parameters based on aerodynamic-theoretical-prediction-algorithms method in order to maximize the target strike area of a missile using grid fins as control devices.

CFD methods proffer a high-fidelity method for computing the aerodynamic parameters of flight vehicles, which could potentially yield more accurate results than theoretical-prediction-methods-when-applied-towards-computing aerodynamic parameters of grid fins. Design methods based on coupling modern numerical optimization algorithms and CFD simulations are favorable methods for grid fins shape design and could potentially lead to improved performance of grid fins design.

Within this paper, grid fins shape is optimized for a launch vehicle based on the coupling of numerical optimization algorithms and CFD simulations. The computational cost of CFD methods could be potentially high. The key point in accomplishing a successful grid fin shape optimization is to increase the efficiency of the optimization methods while reducing the calling times of CFD simulations to as minimal as possible during the optimization procedure. Sequential approximation optimization (SAO) methods are known for their lower computational costs, generality, robustness, and accuracy (Wang and Wu et al., 2014). SAO algorithms require much lesser times for evaluation of original models in order to locate global optimum when compared to evolutionary algorithms (EAs) such as the genetic algorithm (Goldberg, 1989), simulated annealing (Kirkpatrick and Gelatt et al., 1983), particle swarm optimization (PSO) algorithm (Kennedy and Eberhart, 1995), immune algorithm (Yildiz, 2009), and artificial bee colony algorithm (Karaboga and Basturk, 2003), etc. Objectively, SAO algorithms are particularly fit for grid fins shape optimization based on coupling with CFD simulations. Within SAO, the surrogate models are constructed repeatedly by addition of new sampling points, until the terminal criterion is satisfied (Kitayama and Arakawa et al., 2011). Surrogate models construction stage is the most important part of SAO algorithms, and this has been widely studied (Deng and Lam et al., 2002; Kitayama and Arakawa et al., 2011; Kitayama and Yamazaki, 2011; Luo and Zhang et al., 2011). The Radial Basis Function (RBF) model, was originally proposed by Hardy (1971) to fit irregular topographic contours of geographical data. The RBF model has shown to be reliable in terms of accuracy and robustness (Jin and Chen et al., 2001), and is extensively used in SAO algorithms. Determination of the width of an RBF model has decisive impacts on the accuracy of the RBF model (Chen and Hong et al., 2011; Xu and Jayawardena et al., 2013; Yeh and Chen et al., 2012; Wu et al., 2016; Wu et al., 2017; Bonte and Fourment et al., 2010). Nakayama and Arakawa et al. (2002) proposed a determination method of the width for uniform samples. Kitayama and Arakawa et al. (2011) proposed a method for non-uniform and sufficient samples. Wang and Wu et al. (2014) proposed a method based on local densities of sampling points, with the total influence volume as the key parameter for the method, which was obtained by cross validation in a cumbersome approach. Due to the intense non-uniform distribution of samples and progressively increasing samples in an SAO procedure, establishing a reliable RBF width determination method for non-uniform samples with uncertain scale is significantly beneficial for improving the accuracy of surrogate models and the efficiency of SAO algorithms in general.

Multipoint optimization is widely applied in fight vehicles shape optimization (Gallard and Meaux et al., 2013; Lee and Min et al., 2006; Sunago and Sasaki et al., 2009), which means the status of several flights are considered within the optimization procedure. Therefore, within this paper, a multipoint optimization method is employed for grid fins shape optimization for a launch vehicle based on the SAO algorithm and CFD simulations coupling. A new approach for determination of the width of the RBF model is proposed to enhance the RBF surrogate model during the SAO algorithm, and the performance of the proposed method is evaluated. Based on the improved surrogate model, the framework and detailed procedure of the SAO algorithm are presented, and the performance of the proposed SAO algorithm is tested. Weighted average drag coefficients at several selected trajectory points are used as the objective function, and the weighting factors are determined based on strict deducing. The emphasis of obtaining a reasonable objective function is to determine the design trajectory points and the corresponding weighting factors. Constraints are imposed to ensure static stability and controllability for the launch vehicle. Grid fins shape optimization problem of a launch vehicle

is solved using the proposed SAO algorithm, and the optimization results are analyzed and discussed.

2 Radial Basis Function surrogate model and its improvement

In this section, the RBF model is applied to construct the surrogate model. Determination of the width of the basis function is a key factor for establishing an accurate RBF model. Small values of the width leads to a non-smooth regression, while an overly large width value may lead to a Runge's phenomenon in the regression (Wang and Wu et al., 2014). Accurate regression can be obtained with suitable width values. Therefore, based on the local densities of sampling points, an efficient and reliable method to determine the width of basis function is proposed to improve the RBF model for the SAO algorithm.

To deduce the proposed method, an m-dimensional design variable is scaled into an m-dimensional unit hypercube by:

{ } (1)

EMBED Equation.DSMT4

Where { EMBED Equation.DSMT4 } and { EMBED Equation.DSMT4 } are the upper and lower bounds of the { EMBED Equation.DSMT4 } design variable, respectively.

2.1 Standard Radial Basis Function

Given { EMBED Equation.DSMT4 } sampling points { EMBED Equation.DSMT4 }, where { EMBED Equation.DSMT4 } is m-dimensional vector and { EMBED Equation.DSMT4 } is its corresponding real response value, the standard RBF model has the general form of:

{ } (2)

EMBED Equation.DSMT4

Where { EMBED Equation.DSMT4 } is the vector of design variables, { EMBED Equation.DSMT4 } is a vector value of the { EMBED Equation.DSMT4 } sampling point, { EMBED Equation.DSMT4 }is the Euclidean norm, { EMBED Equation.DSMT4 } is the coefficient for the { EMBED Equation.DSMT4 } basis function, and { EMBED Equation.DSMT4 } is a basis function. The following Gaussian kernel is employed as the basis function in this paper:

{ } (3)

EMBED Equation.DSMT4

Where { EMBED Equation.DSMT4 } is the width of the { EMBED Equation.DSMT4 } basis function, and { EMBED Equation.DSMT4 } should be determined before the calculation of { EMBED Equation.DSMT4 }.

The response { EMBED Equation.DSMT4 }$\psi$is calculated using Eq. (2) at sampling point { EMBED Equation.DSMT4 }.ψThe calculation of { EMBED Equation.DSMT4 } is performed by solving the following equation:

{ EMBED Equation.DSMT4 } (4)

Eq. (4) can be re-written as:

{ EMBED Equation.DSMT4 } (5)

Where,

{ } (6)

EMBED Equation.DSMT4

And { EMBED Equation.DSMT4 }, { EMBED Equation.DSMT4 }.

Nakayama proposed a simple manner to determine the width of the basis functions as follows (Nakayama and Arakawa et al., 2002):

{ } (7)

EMBED Equation.DSMT4

Where { EMBED Equation.DSMT4 } represents the maximum distance between the sampling points. In an m-dimensional unit hyper-cube, the upper bound of { EMBED Equation.DSMT4 } is clearly { EMBED Equation.DSMT4 }. { EMBED Equation.DSMT4 } in Eq. (7) is replaced with { EMBED Equation.DSMT4 }, therefore, we can get:

{ } (8)

EMBED Equation.DSMT4

Eq. (7) leads to a constant width value for every basis function. If the training data are non-uniformly distributed as most practical problems show, it is expected that this kind of method may not work well. Kitayama and Arakawa et al. (2011) proposed the following simple determination which attempts to deal with the non-uniform distribution of sampling points.

{ } (9)

EMBED Equation.DSMT4

Where { EMBED Equation.DSMT4 } denotes the width of the { EMBED Equation.DSMT4 } Gaussian kernel and { EMBED Equation.DSMT4 } denotes the maximum distance between the { EMBED Equation.DSMT4 } sampling point and other sampling points.

2.2 *Determination of the width of the RBF model*

2.2.1 *Determination method*

Intuitively, widths of the basis functions should be closely related with sampling points distribution density. The denser, the smaller the width. Kernel density estimation function (KDE) is a wildly used method for sample densities estimation (Parzen, 1962). According to KDE, the density function is defined as follows while applying Gaussian kernel;

{ } (10)

EMBED Equation.DSMT4

The density function of one-dimensional random sample with respect to { EMBED Equation.DSMT4 } is illustrated in Fig. 1. An appropriate value of { EMBED Equation.DSMT4 } is needed to reveal the distribution densities accurately, while a small { EMBED Equation.DSMT4 } value leads to impulse function, and an overly large { EMBED Equation.DSMT4 } value leads to a density function reflecting no local distribution features.

In this paper, { EMBED Equation.DSMT4 } in Eq. (10) takes the form of Eq. (8). The local density of the sampling point { EMBED Equation.DSMT4 } is defined as follows:

{ } (11)

EMBED Equation.DSMT4

In Fig. 1., there are 23 sampling points, as shown in Fig. 2. Setting { EMBED Equation.DSMT4 } leads to reasonable local density values for sampling points.

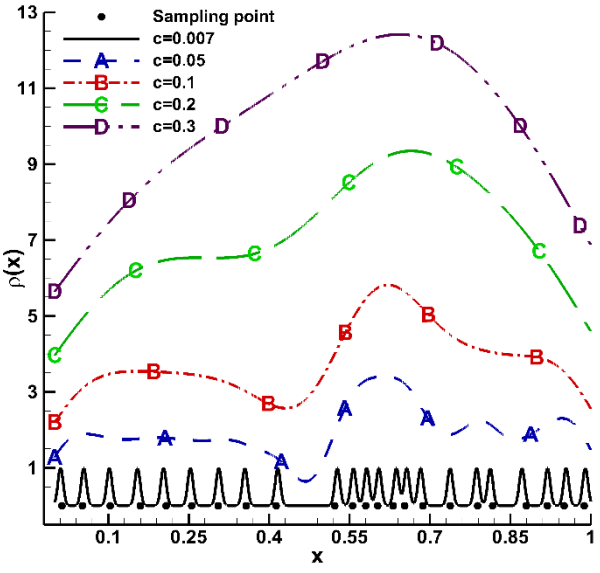

Fig. 1. Density function of one-dimension random sample with respect to { EMBED Equation.DSMT4 }

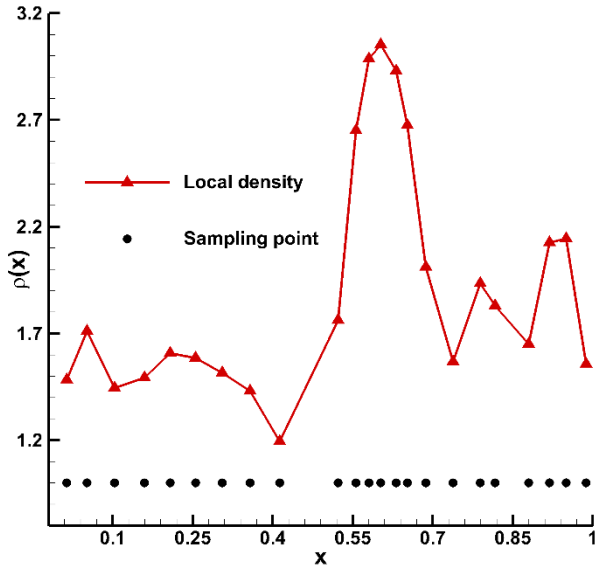

Fig. 2. Local densities of one-dimension sampling points

The relationship between the width of the { EMBED Equation.DSMT4 } basis function { EMBED Equation.DSMT4 } in Eq. (3), { EMBED Equation.DSMT4 } and design space dimension { EMBED Equation.DSMT4 } can be expressed as:

{ } (12)

EMBED Equation.DSMT4

Eq. (12) contains { EMBED Equation.DSMT4 } mutual independent equations, and the number of unknown width { EMBED

{ EMBED Equation.DSMT4 } needed to solve is { EMBED Equation.DSMT4 }. All { EMBED Equation.DSMT4 } could be obtained if whichever { EMBED Equation.DSMT4 } is determined reasonably.

The sparsest sample point { EMBED Equation.DSMT4 } is taken as a breakthrough for { EMBED Equation.DSMT4 } determination. To ensure smooth regression, basis function { EMBED Equation.DSMT4 }'s influence should reach its nearest sample point, that is; basis function value of { EMBED Equation.DSMT4 } at its nearest sample point should be great enough.

{ } (13)

EMBED Equation.DSMT4

Where { EMBED Equation.DSMT4 } denotes the minimum distance between the sparsest sampling point and other sampling points, { EMBED Equation.DSMT4 } denotes the width of the sparsest sampling point. The numerical relationship between { EMBED Equation.DSMT4 } and { EMBED Equation.DSMT4 } is illustrated in Fig. 3. { EMBED Equation.DSMT4 } is less than 0.1 while { EMBED Equation.DSMT4 } is less than 0.6592, and { EMBED Equation.DSMT4 } is greater than 0.3769 while { EMBED Equation.DSMT4 } is greater than 1.0. Setting { EMBED Equation.DSMT4 } should be sensible to ensure smooth regression, in other words, { EMBED Equation.DSMT4 } could be calculated as follows:

{ EMBED Equation.DSMT4 } (14)

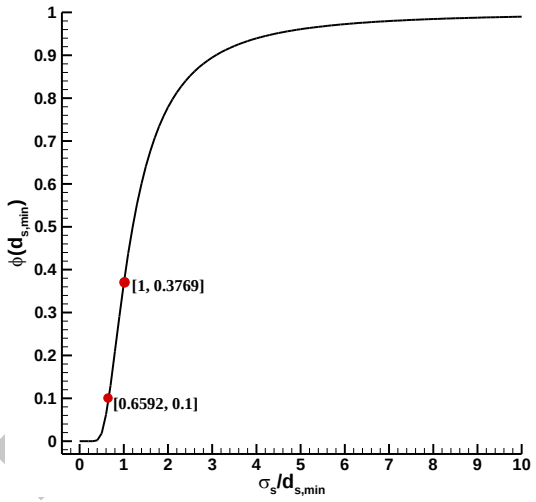

Fig. 3. The numerical relationship between { EMBED Equation.DSMT4 } and { EMBED Equation.DSMT4 }

According to Eq. (12) and Eq. (14), width { EMBED Equation.DSMT4 } estimation method is proposed as follows:

{ EMBED Equation.DSMT4 } (15)

2.2.2 Method Evaluation

The approximation accuracy of the proposed method and the methods given by Nakayama & Arakawa et al. (2002) and Kitayama & Arakawa et al. (2011) are further assessed by the index of R-squared ({ EMBED Equation.DSMT4 }), depicted as follows;

{ } (16)

EMBED Equation.DSMT4

Where { EMBED Equation.DSMT4 } is the number of validation sample, { EMBED Equation.DSMT4 } is the observed value, { EMBED Equation.DSMT4 } is the approximated value, { EMBED Equation.DSMT4 } is the average of all observed values. The closer{ EMBED Equation.DSMT4 }is to 1, the more precise the surrogate model. { EMBED Equation.DSMT4 } means no associated error between observed and approximated values.

Five functions shown in Tab. 1. are chosen to assess approximation accuracy of these three methods. With regards to function 1, comparisons of the three methods are illustrated in Fig. 4. and Fig. 5. As shown in Fig. 4., the proposed method performs much better than the methods given by Nakayama and Kitayama when the eight sampling points are non-uniform, where{ EMBED Equation.DSMT4 }values of the three methods are 0.995, 0.655 and 0.517 respectively. In Fig. 5., when the eight sampling points

are uniform, the { EMBED Equation.DSMT4 } values of the three methods are 0.966, 0.939 and 0.922 respectively, with the proposed method constantly out performing the other two methods.

To evaluate the efficacy and efficiency of the proposed width determination method more thoroughly, a special validation procedure presented by Wang and Hu et al. (2014) is applied. In the procedure, 10 random points are sampled each time for function 1, 50 random points for function 2 and function 3, 200 random points for function 4 and function 5 are all sampled randomly each time. The RBF surrogate models corresponding to the three test width determination methods are obtained. 1000 points are selected to calculate { EMBED Equation.DSMT4 } between the surrogate models and the true function. The whole process repeats independently for 20 times, and the mean { EMBED Equation.DSMT4 } ({ EMBED Equation.DSMT4 }) is calculated.

Tab. 1. Test functions for approximation accuracy evaluation

Function	Function expression	Notes
Function 1	{ EMBED Equation.DSMT4 }	One-dimension function
Function 2	{ EMBED Equation.DSMT4 }	Low dimension and low order function
Function 3	{ EMBED Equation.DSMT4 }	Low dimension and high order function
Function 4	{ EMBED Equation.DSMT4 }	High dimension and low order function
Function 5	{ EMBED Equation.DSMT4 }	High dimension and high order function

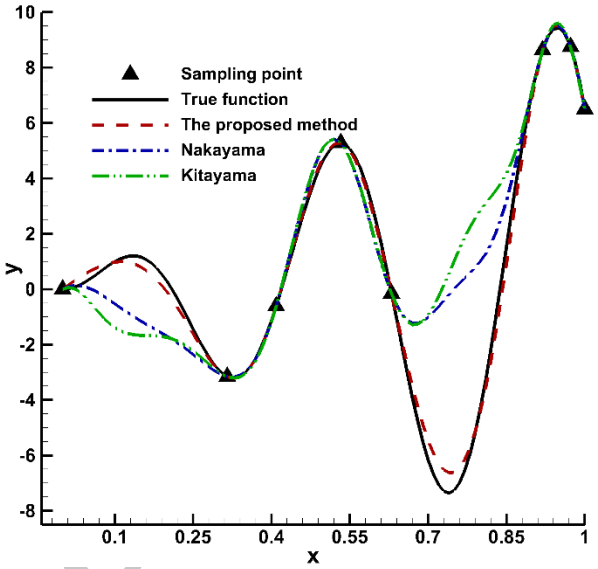

Fig. 4. Comparison of the approximation performance with respect to 8 non-uniform sampling points

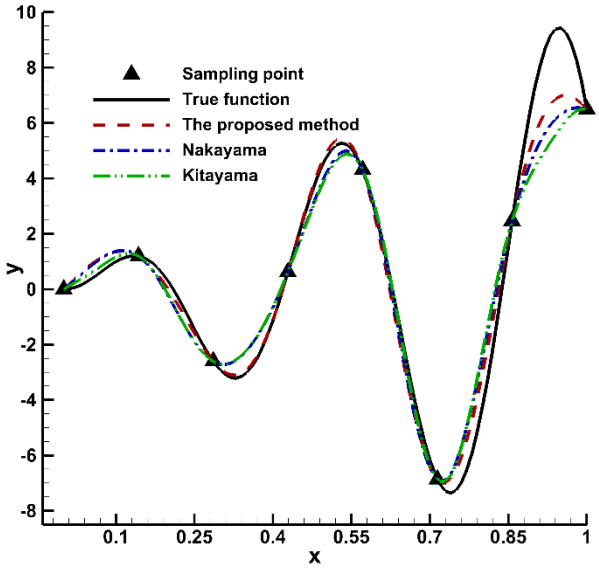

Fig. 5. Comparison of the approximation performance with respect to 8 uniform sampling points

The approximation accuracy corresponding to the three test width determination methods are illustrated in Fig. 6. The proposed method shows the best performance for all five test functions, Nakayama's method takes the second place. With regards to the higher dimension functions (function 4 and function 5), the proposed method demonstrates much superior performance when compared to the Nakayama and Kitayama methods.

The fluctuations of { EMBED Equation.DSMT4 } for each function when using the three width determination methods are further illustrated in Fig. 7. The { EMBED Equation.DSMT4 } values of the proposed method are constantly greater than 0.9 in most random validation cases even for the high dimension and high order function (function 5). The { EMBED Equation.DSMT4 } values of the proposed method are greater than Nakayama's and Kitayama's method in almost all cases. Also, its { EMBED Equation.DSMT4 } fluctuations are much steadier than the other two methods.

In particular, the main calculation cost of this proposed width determination method is calculating { EMBED Equation.DSMT4 }

in Eq. (11), and fortunately, { EMBED Equation.DSMT4 } is also needed while solving Eq. (4). Therefore, this proposed method for width determination generates almost no excessive calculation costs. Generally, this proposed determination method of width for the RBF model has an accurate, reliable and stable performance.

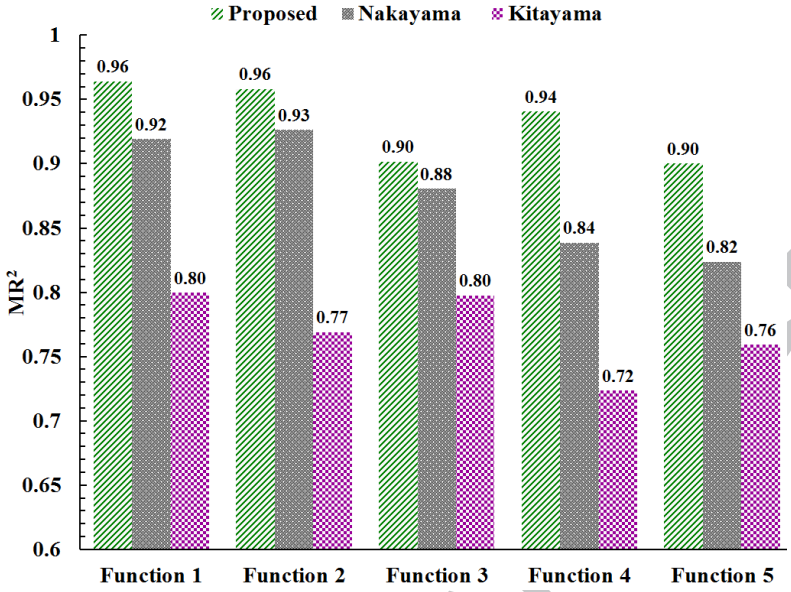

Fig. 6. Comparison of approximation accuracy corresponding three width determination methods by the index of { EMBED Equation.DSMT4 }

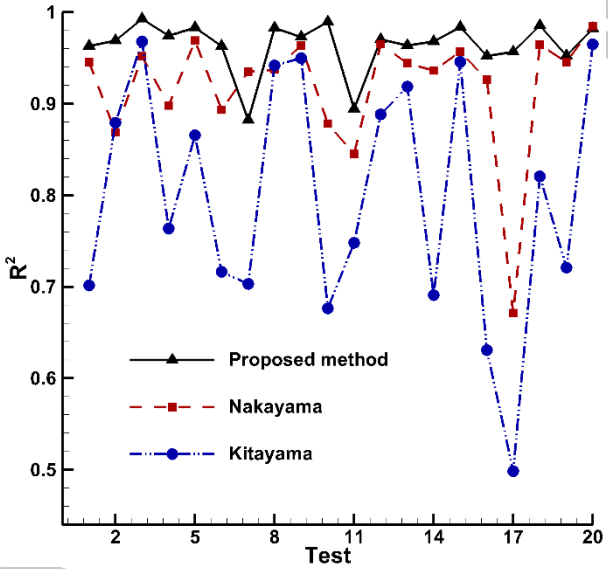

(a) Function 1

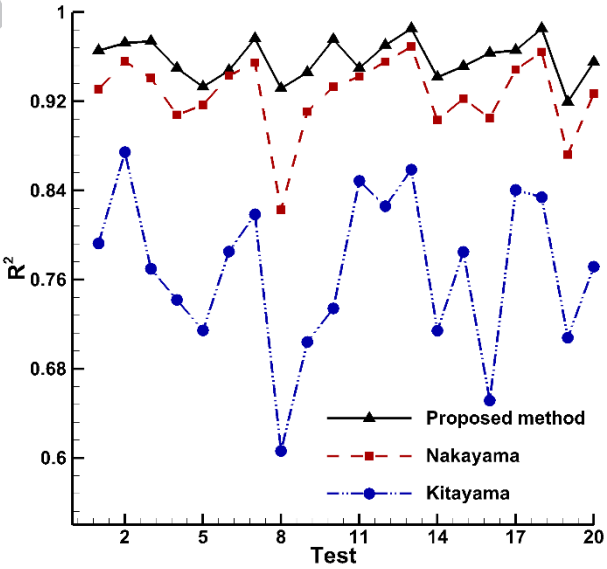

(b) Function 2

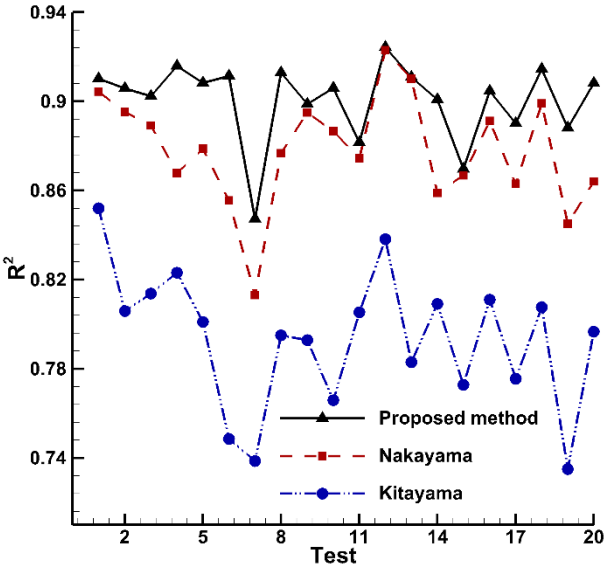

(c) Function 3

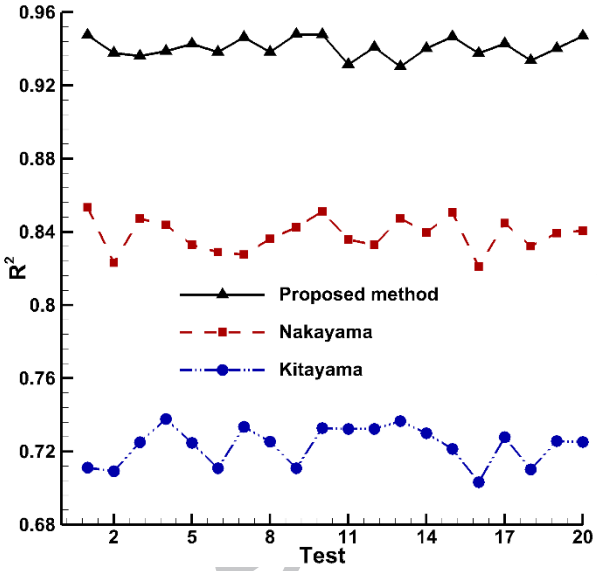

(d) Function 4

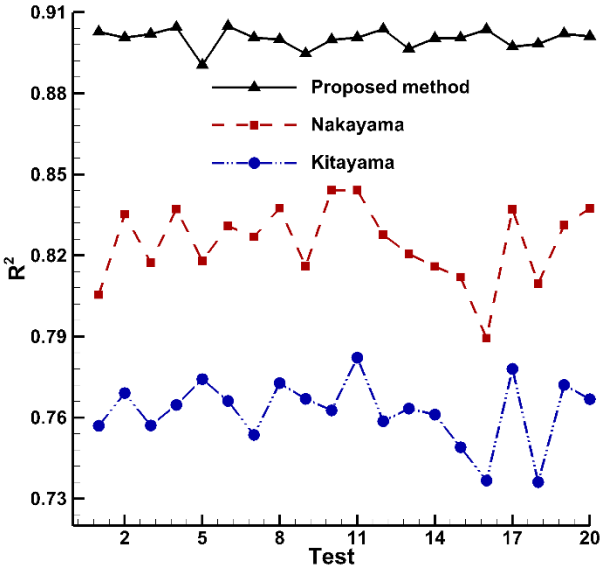

(e) Function 5

Fig. 7. The fluctuations of { EMBED Equation.DSMT4 } in the validation procedure

3 SAO algorithm based on the improved RBF surrogate model

3.1 Algorithm

For convenience of discussion, expression of the ordinary optimization problem is given as follows:

{ } (17)

EMBED Equation.DSMT4

Where { EMBED Equation.DSMT4 }, { EMBED Equation.DSMT4 }, { EMBED Equation.DSMT4 } are the objective function, inequality constraints, and equality constraint respectively.

The framework of the SAO algorithm utilized in this paper is presented in Fig. 8. The detailed procedure of the SAO algorithm utilized is broadly divided into the initial stage, approximation stage, and sampling stage, which are elaborated as follows:

(1) Initial stage

In this stage, the m-dimensional design variable is first scaled into an m-dimensional unit hypercube, then the Optimal Latin Hypercube Design (OLHD) method is used to sample the unit hypercube. The objective function and constraints of the sampling

points are then evaluated using the original model. The sampling points and the corresponding responses constitute the initial sample set.

(2) Approximation stage

Based on the sample set, surrogate models of the objective function and the constraints are constructed using the improved RBF model. The local densities of sampling points are calculated, then width of the basis function of the sparsest sample point is calculated, after which the widths of basis functions of other sample points are determined. Finally, accuracy of the RBF surrogate models are constructed based on the efficiently and reliably determined widths of basis functions.

(3) Sampling stage

Since the advent and introduction of the SAO algorithm, a number of sampling strategies have been studied and applied (Hastie and Tibshirani et al., 2001; Jones, 2001; Xiong and Chen et al., 2007). These strategies can be divided into three categories: the exploitation technique, the exploration technique, and the balanced exploitation/exploration technique. An adaptive sampling strategy of solving the following optimization problem with a penalty method is used in this paper in order to balance the exploitation and exploration (Wang and Wu et al., 2014).

{ **}** (18)

EMBED Equation.DSMT4

Where **{** EMBED Equation.DSMT4 **}**, **{** EMBED Equation.DSMT4 **}**, **{** EMBED Equation.DSMT4 **}** are the surrogate models of objective function, inequality constraints, and equality constraint respectively, **{** EMBED Equation.DSMT4 **}** is the minimum Euler distance between the new sampling point and the former sampling points, **{** EMBED Equation.DSMT4 **}** is the minimum distance between the existing sampling points, and **{** EMBED Equation.DSMT4 **}** will decrease gradually in the SAO iteration procedure.

In the sampling stage, the minimum distance **{** EMBED Equation.DSMT4 **}** between the sampling points in the sample set is initially calculated, and then, based on the surrogate models constructed in the approximation stage, the adaptive sampling is implemented by solving the optimization problem (18) using the PSO algorithm with a penalty method. Finally, the optimal solution, together with its objective function and constraints of the original model, are added to the sample set to update the surrogate models in the next iteration.

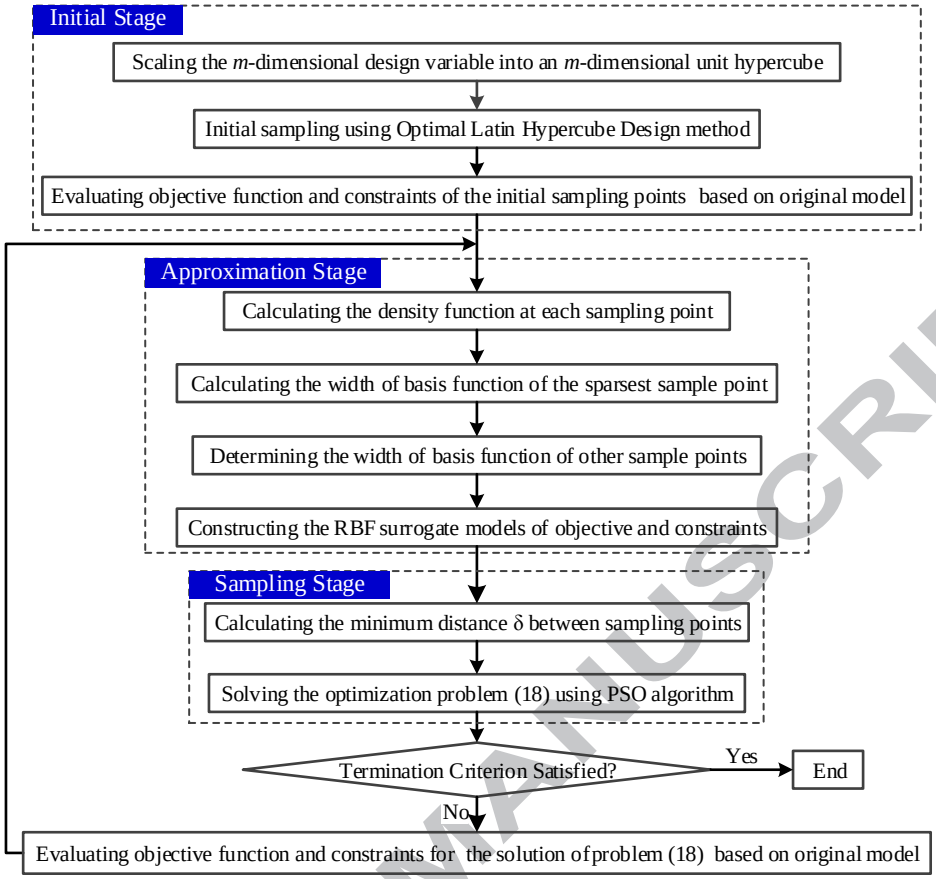

Fig. 8. The framework of the SAO algorithm.

3.2 Algorithm test

The Golinski's speed reducer problem is a classical and widely used optimization algorithm testing problem, which is also included in the MDO test suite at NASA Langley Research Center (Padula and Alexandrov et al., 1996). The mathematical expression of the Golinski's speed reducer problem is as follows:

{ } (19)

EMBED Equation.DSMT4

Where,

{ }

EMBED Equation.DSMT4

{ }

EMBED Equation.DSMT4

The respective maximum and minimum bounds of design variables for the Golinski's speed reducer problem is:

{ } (20)

EMBED Equation.DSMT4

Where { EMBED Equation.DSMT4 } is an integer.

20 initial sampling points are generated using OLHD method. As shown in Fig. 9., the global optimal solution is obtained after 35 iterations, while the original model is called 65 times. The optimal solution is:

{ EMBED Equation.DSMT4 } (21)

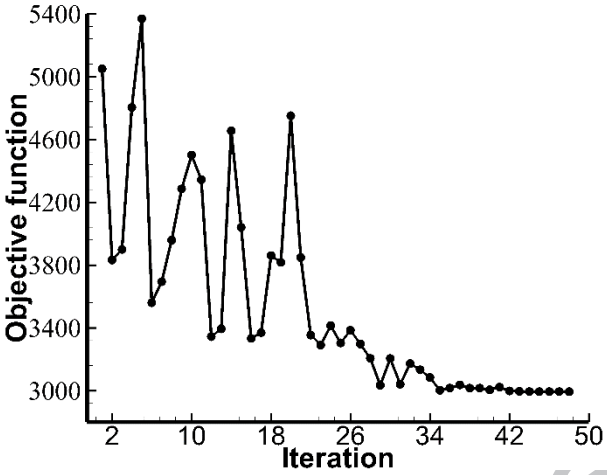

Fig. 9. The objective function history of the optimization process for Golinski's speed reducer problem

The parallel simulated annealing algorithm using simplex method (PSASM) proposed by Luo and Tang (2004) is an acknowledged excellent optimization algorithm. The optimal solution for Golinski's speed reducer problem is obtained after calling the original model about 1000 times using PSASM. In contrast, the proposed SAO algorithm can reduce the calling times of the original model and improve the optimization efficiency notably. Therefore, grid fins shape optimization of a launch vehicle based on CFD simulations could be achieved efficiently using the proposed SAO algorithm.

4 Grid fins shape design optimization of a launch vehicle

4.1 Conceptual design of the launch vehicle

The launch vehicle is a three-stage solid rocket, the mass of load-to-orbit (including mass of payload, payload adapter and burnt-out last stag) is 250 kilograms, and payload mass is 50 kilograms. Orbit altitude of satellite is 300 kilometers. Four grid fins are installed in the shape of a cross as aerodynamic stabilizing surface and aerodynamic control rudder of the first stage. The baseline shape of the launch vehicle is shown in Fig. 10. Chord length of grid fins is 120 millimeters, distance between neighboring internal webs is 158.4 millimeters, height of the fin support base is 100 millimeters, distance between the grid fins and rocket bottom is 150 millimeters, number of cells are 3 in both span-wise direction and the perpendicular direction of span-wise direction, outer web thickness is 8 millimeters, internal web thickness is 5 millimeters, and the internal webs of grid fins are orthogonal.

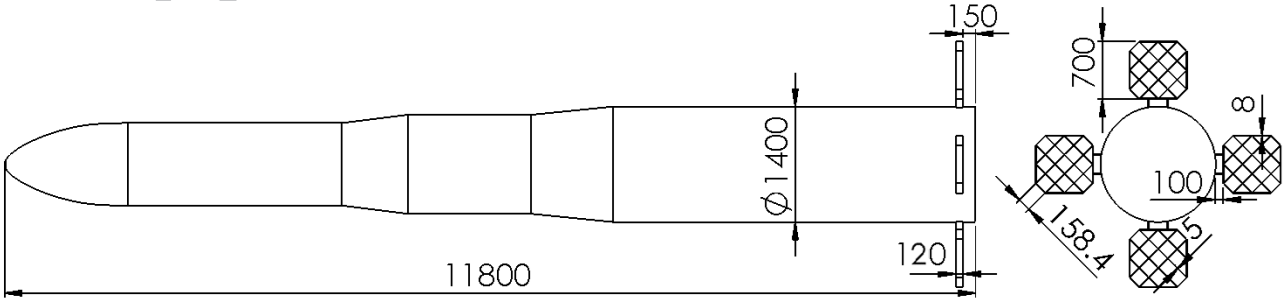

Fig. 10. Baseline configuration of a launch vehicle

The minimum fuel trajectory is obtained using the method of Hu and Yang et al. (2010). Fig. 11. shows the altitude, Mach number and velocity vs. time curves of the minimum fuel trajectory. Mach numbers up to 100 km have no physical meaning, which are not illustrated in Fig. 11. Fig. 12. shows the slope angle and dynamic pressure vs time curves of the minimum fuel trajectory. The take-off mass corresponding the minimum fuel trajectory is 14.58 tons.

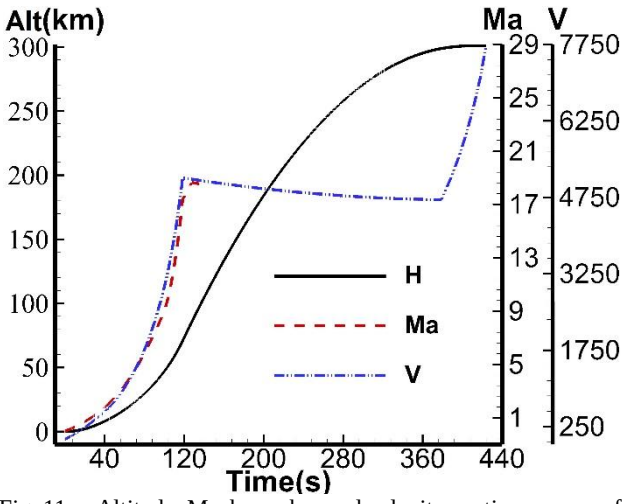

Fig. 11. Altitude, Mach number and velocity vs. time curves of the minimum fuel trajectory

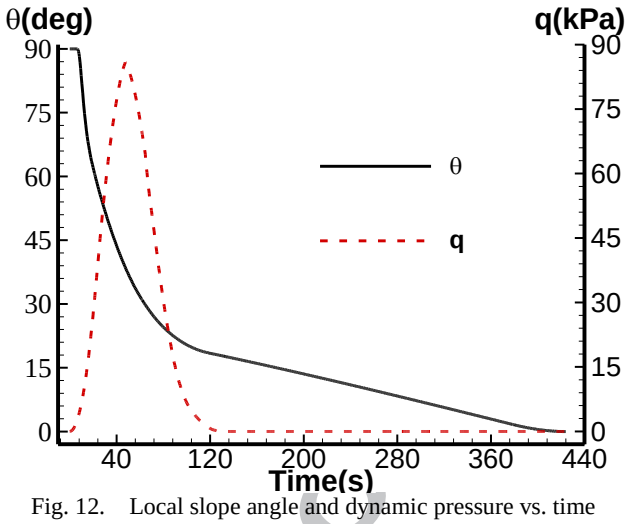

Fig. 12. Local slope angle and dynamic pressure vs. time curves of the minimum fuel trajectory

4.2 Design variables of grid fins for the launch vehicle

The four parameters selected as design variables for the grid fins shape optimization are: (1) Chord length of the grid fins ({ EMBED Equation.DSMT4 }), (2) Distance between neighboring internal webs ({ EMBED Equation.DSMT4 }), (3) Height of the grid fins support base ({ EMBED Equation.DSMT4 }), (4) Number of cells in span-wise direction and the perpendicular direction of span-wise direction ({ EMBED Equation.DSMT4 }). The first three parameters can be seen in Fig. 13. The design variables can be represented as follows:

$$\{\ \text{EMBED Equation.DSMT4}\ \} \tag{22}$$

{ EMBED Visio.Drawing.15 }

Fig. 13. Design variables of grid fins for the launch vehicle

The maximum and minimum bounds of design variables for grid fins are determined according to experiences in this study, and the range is chosen large enough to ensure the global optimal solution within limits. The respective maximum and minimum bounds are shown in Tab. 2.

Tab. 2. The respective maximum and minimum bounds of design variables for grid fins

Parameters	Minimum Limit	Maximum Limit
{ EMBED Equation.DSMT4 }/mm	80	200
{ EMBED Equation.DSMT4 }/mm	90	180
{ EMBED Equation.DSMT4 }/mm	50	200
{ EMBED Equation.DSMT4 }	2	5

4.3 Objective function and constraints

As aerodynamic stabilizing surface and aerodynamic control rudder of the first stage within launch vehicles, the grid fins should satisfy requirements of static stability and controllability, and also cause least aerodynamic drag.

4.3.1 Objective function

Weighted average drag coefficients at several selected trajectory points are used as the objective function by many researchers (Kenway and Martins, 2016; Lee and Min et al., 2006; CHAI and YU et al., 2018). The emphasis of obtaining a reasonable objective function is to determine the design trajectory points and the corresponding weighting factors. This paper proposes a method for obtaining a reasonable objective function, which is deduced as follows;

The direct purpose of decreasing the aerodynamic drag in grid fins shape optimization process is to reduce the momentum loss caused by drag, which is expressed by the following formulation:

{ EMBED Equation.DSMT4 } (23)

Where { EMBED Equation.DSMT4 } is the separation moment between the first stage and the second stage, { EMBED Equation.DSMT4 } is the aerodynamic drag, { EMBED Equation.DSMT4 } is drag coefficient, { EMBED Equation.DSMT4 } is dynamic pressure, { EMBED Equation.DSMT4 } is the reference area of { EMBED Equation.DSMT4 }, the value { EMBED Equation.DSMT4 } is set to make { EMBED Equation.DSMT4 }, so as to ignore the almost zero dynamic pressure flight process after { EMBED Equation.DSMT4 }.

Dividing the time interval { EMBED Equation.DSMT4 } to { EMBED Equation.DSMT4 } parts uniformly, Eq. (23) could be transformed as:

{ EMBED Equation.DSMT4 } (24)

Where { EMBED Equation.DSMT4 } is the drag coefficient at the { EMBED Equation.DSMT4 } moment. Dividing by { EMBED Equation.DSMT4 }, Eq. (24) could be transformed as:

{ EMBED Equation.DSMT4 } (25)

Where:

{ EMBED Equation.DSMT4 } (26)

The value of { EMBED Equation.DSMT4 } wouldn't change obviously after the grid fins shape optimized, because the variation of aerodynamic drag between optimized grid fins and baseline configuration has slight influence on dynamic pressure vs. time.

Based on the above derivation, this paper proposes the following objective function for grid fins shape optimization.

{ EMBED Equation.DSMT4 } (27)

The objective function expressed by Eq. (27) reflects the momentum loss caused by drag directly, and is beneficial for satisfactory grid fin shape optimizations.

The value of { EMBED Equation.DSMT4 } in Eq. (27) is set as 3, which results to the design trajectory points and corresponding weighting factors shown in Tab. 3. for the objective function. In Tab. 3., The angle of attack { EMBED Equation.DSMT4 } and grid fins deflection angles is set to 10° and 0° for calculation of { EMBED Equation.DSMT4 }, { EMBED Equation.DSMT4 } is the distance between the center of mass and the nose vertex, { EMBED Equation.DSMT4 } is the total length of the launch vehicle.

Tab. 3. Design trajectory points and the corresponding weighting factors for the objective function

{ EMBED Equation.DS	10.30	30.91	51.51

{ EMBED Equation.DSMT4 }/s			
{ EMBED Equation.DSMT4 }/km	0.55	4.92	12.83
{ EMBED Equation.DSMT4 }/kPa	6.99	58.77	82.75
{ EMBED Equation.DSMT4 }	0.32	1.24	2.64
{ EMBED Equation.DSMT4 }	0.07	0.39	0.55
{ EMBED Equation.DSMT4 }	0.57	0.5	0.45

4.3.2 Constraints

The following constraints are imposed to ensure static stability and controllability for the launch vehicle.

(1) The static margin at the design trajectory points in Tab. 3. should be greater than 0.03, to meet the requirement of static stability;

{ EMBED Equation.DSMT4 } (28)

Where { EMBED Equation.DSMT4 } is the distance between the aerodynamic center and the nose vertex at the three selected design trajectory points.

(2) The absolute value of desired deflection angles { EMBED Equation.DSMT4 } needed to trim the launch vehicle at the design trajectory points in Tab. 3. should be smaller than 15°, while the angle of attack { EMBED Equation.DSMT4 } is set as 10 degrees, so as to meet the controllability requirement.

{ EMBED Equation.DSMT4 } (29)

Where { EMBED Equation.DSMT4 } is calculated as follows:

{ } (30)
EMBED Equation.DSMT4

Where { EMBED Equation.DSMT4 } is pitching moment, and { EMBED Equation.DSMT4 } is the deflection angle of grid fins.

(3) Setting angle of attack and grid fins deflection angles to zero and 20°, the absolute value of hinge moment at the design trajectory points in Tab. 3. should be smaller than 250 { EMBED Equation.DSMT4 }, so as to lower the output torque requirements of the actuator.

{ EMBED Equation.DSMT4 } (31)

In summary, six independent numerical simulations at { } and { } for
EMBED Equation.DSMT4 EMBED Equation.DSMT4
three design trajectory points are needed to calculate the objective function and constraints.

4.4 Results and Discussion

Based on the proposed SAO algorithm of Section 3, the objective function and constraints calculation tasks are accomplished in batch mode automatically by taking three steps as follows:

Step 1: The rocket shape is modeled according to the values of design variables using SolidWorks macro tool automatically.

Step 2: Structured-unstructured hybrid meshes for external flow-field simulations are made using ANSYS ICEM CFD 16.1 script tool automatically. As the external flow-field is symmetrically distributed, half of the outer flow-field is needed for mesh generation, and the meshes on symmetry and grid fin are as shown in Fig. 14. The total mesh cells of the flow domain are about 3.2 million. It is worth mentioning that only the unstructured meshes around the grid fins are required to be made during the optimization process, while the region of structured meshes remains unchanged during optimization, thereby saving time.

Step 3: Numerical simulation of outer flow-fields of the rocket at every attack angle, deflection angle and design trajectory point are completed using ANSYS Fluent 16.1 running in batch mode, with the Spalart-Allmaras (S-A) turbulence model adopted. The objective function and constraints are solved by post-processing the rockets outer flow-field numerical simulation results.

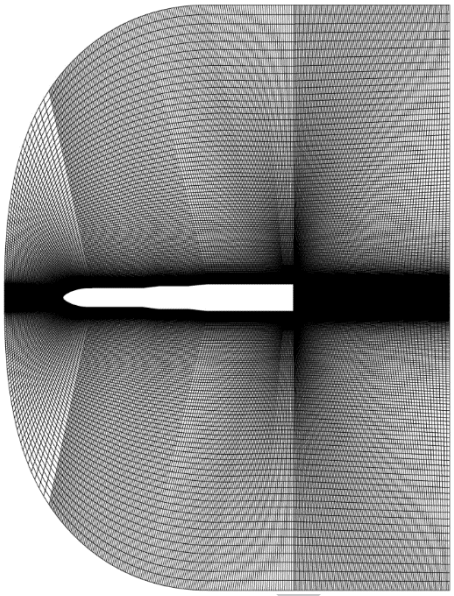

(a) Meshes of symmetry plane

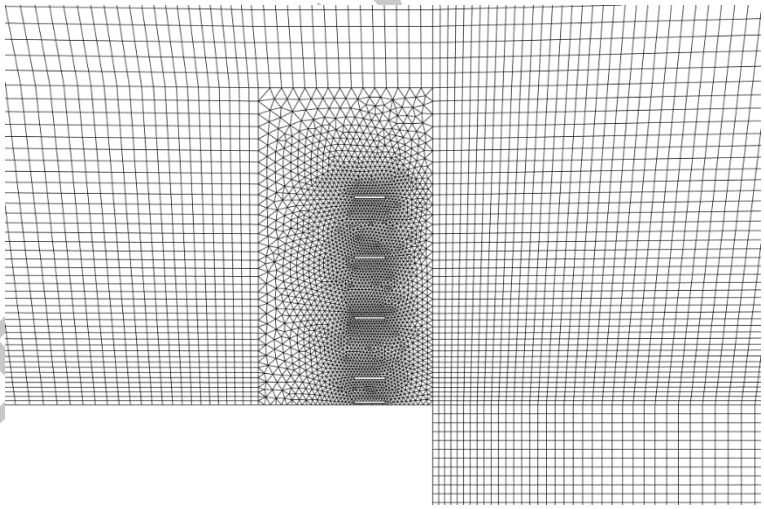

(b) Local magnifying meshes of symmetry plane around a grid fin

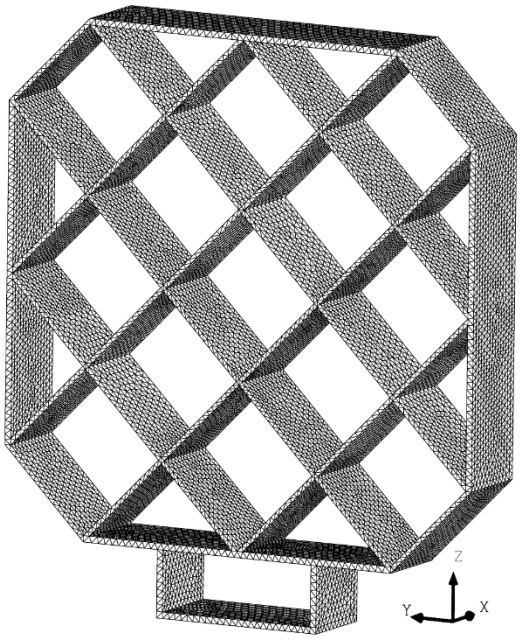

(c) Surface meshes of a grid fin

Fig. 14. The computational meshes of the rocket with grid fins

The accuracy of the CFD method performed in this paper is tested using wind tunnel test data (Theerthamalai and Nagarathinam et al., 2006) of a rocket model with grid fins shown in Fig. 15. The Mach number of the wind tunnel test is 2.5, and the Reynolds number is 1.2×10^6 based on the diameter of the rocket model, the angle of attack is 0 to 24 degrees. The coefficient of drag, lift coefficient, and pitch moment coefficient calculated using ANSYS ICEM CFD 16.1 and Fluent 16.1 are compared with the wind tunnel test results. The aerodynamic coefficients reference length is the length of the rocket model, the reference area is the maximum sectional area of the rocket body, and the nose vertex is taken as the aerodynamic moment reference point. It can be seen from Fig. 16. that the calculated results of aerodynamic coefficients are in good agreement with the test results, with the error between calculated and test results of drag coefficient { EMBED Equation.DSMT4 }, lift coefficient { EMBED Equation.DSMT4 } and pitching moment { EMBED Equation.DSMT4 } all less than 6.5%, 4.9%, and 4.7% respectively.

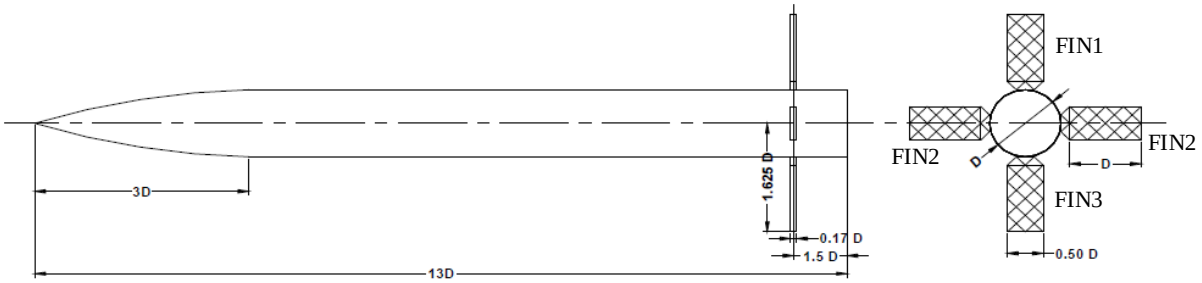

Fig. 15. Rocket model with grid fins

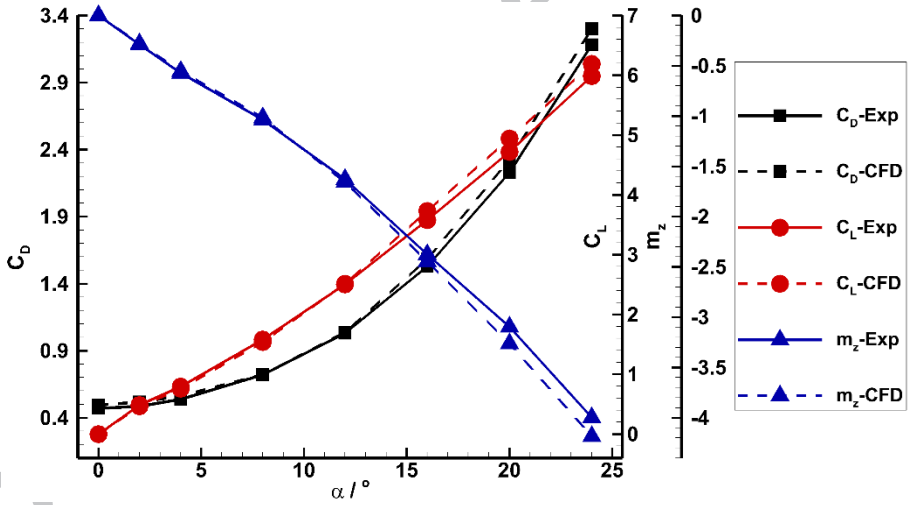

Fig. 16. The comparison of calculated and test results of aerodynamic characteristics of rocket model with grid fins

15 initial sampling points are generated using OLHD method for the grid fins shape optimization. The objective function history of the grid fins optimization process is shown in Fig. 17. The objective function becomes stable after 39 iterations, thereby producing the global optimal solution after 39 iterations; while the original model is called 54 (15 plus 39) times.

Computational time of 83 minutes is taken to compute the objective function and constraints of a specified configuration in our computing cluster possessing 96 cores. 92 hours (3.84 days) is taken altogether to obtain the optimal grid fins shape for the rocket using the proposed SAO algorithm. Assuming evolutionary algorithms are used to solve the optimization problem of grid fins performed in this paper, the original model will be called thousands of times, and much more expensive consumption times would be required, which is often difficult to accept in most engineering projects.

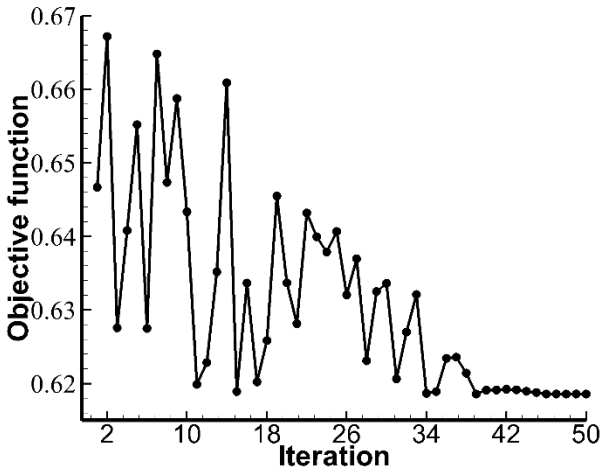

Fig. 17. The objective function history of the optimization process for grid fins

Optimized Grid Fins Geometry Parameters are as shown in Tab. 4. Shape of the launch vehicle with optimized grid fins is as shown in Fig. 18.

Tab. 4. Optimized grid fins geometry parameters

Parameters	{ EMBED Equation.DSMT4 }/mm	{ EMBED Equation.DSMT4 }/mm	{ EMBED Equation.DSMT4 }/mm	{ EMBED Equation.DSMT4 }
Optimized Value	97.26	129.52	75.48	3

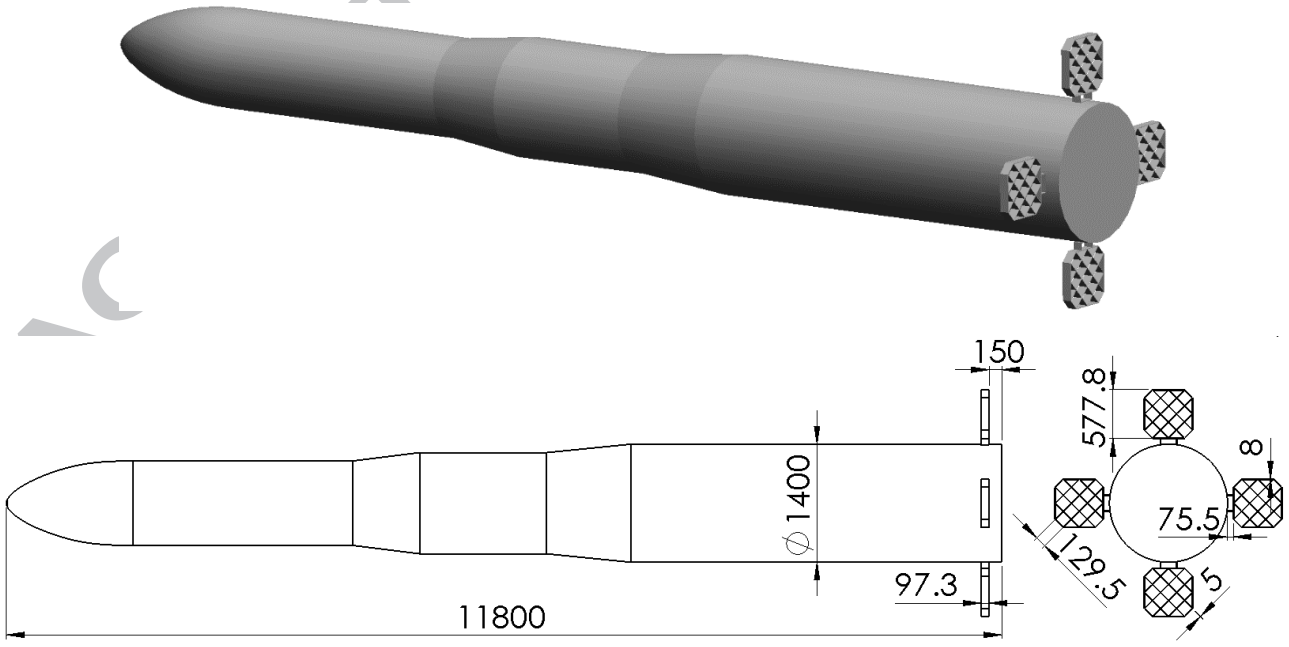

Fig. 18. Shape of launch vehicle with optimized grid fins

Flow parameters contour (taking the free stream of Mach 2.64, angle of attack and grid fins deflection angles is equal to 10° and 0°, for example) of the rocket with grid fins optimized are shown in Fig. 19. Strong local oblique shock waves pass through the fin cells,

and the flow remains supersonic within the cells, which means there are no existence of flow choking.

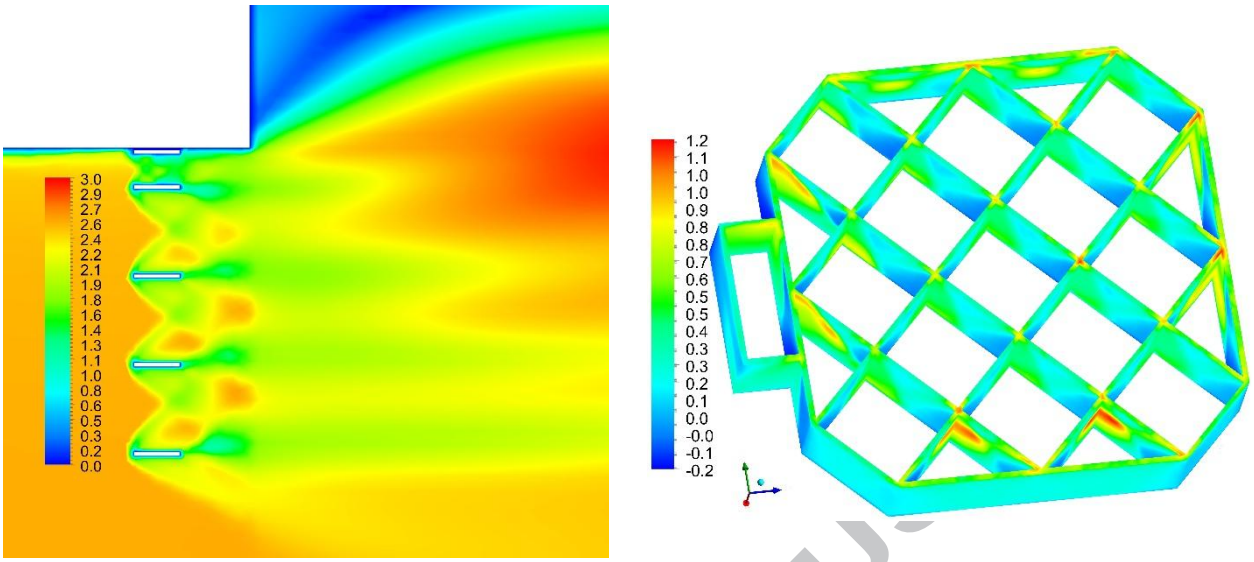

(a) Mach number contours around the windward grid fin on the symmetry

(b) Pressure coefficient contours of the horizontal grid fin

Fig. 19. Flow parameters contours at free stream of Mach 2.64, angle of attack and grid fins deflection angles is equal to 10° and 0°

The objective functions and constraints of the baseline shape and the optimized shape are as shown in Tab. 5. The optimal solution satisfies all constraint conditions initially presented in section 4.3.2, and the weighted average drag coefficient as the objective function achieved in this paper is 11.07% less than the value of the baseline shape, which is beneficial for improving launch performance of launch vehicles.

Tab. 5. Objective functions and constraints of the baseline shape and the optimized shape

Launch vehicle shape	{ EMBED Equation.DSMT4 }	{ EMBED Equation.DSMT4 }	{ EMBED Equation.DSMT4 }	{ EMBED Equation.DSMT4 }
The baseline shape	0.6956	0.035	-5.7	-26.5
The optimized shape	0.6186	0.00091	-4.54	-45.6

Adopting the analysis approach given by Hu and Yang et al. (2010), by replacing the baseline shape with the optimized shape, it is observed that; (1) taking the minimum fuel as an objective function for optimization, the take-off mass will be 14.274 tons, which is 301.71 kilograms and 2.07% lighter than the take-off mass of the baseline shape, (2) taking the maximum payload mass as an objective function for optimizing, the payload mass will be 57.1 kilograms, which is 7.1 kilograms and 14.2% heavier than the payload mass of the baseline shape.

5 *Conclusion*

Grid fins shape is optimized for a launch vehicle based on the SAO algorithm and CFD simulations. The main work and conclusion of this study are as follows:

(1) An efficient and reliable method is proposed to determine the width of Gaussian functions. Based on the local densities of sampling points, the basis function width of the sparsest sample point is calculated reasonably, and then the basis function widths of other sample points are determined according to the logical relationship between the width and local density. The performance of this proposed method is evaluated using five classical test functions. The proposed method for width determination generates almost no

excessive calculation costs, and improves the accuracy, reliability, and stability of the RBF surrogate models notably.

(2) Based on the improved surrogate model, the framework and detailed procedure of the SAO algorithm are presented. The performance of the proposed SAO algorithm is tested using the Golinski's speed reducer problem. The test shows that the proposed SAO algorithm reduces the calling times of the original model and improves the optimization efficiency remarkably.

(3) The objective function is strictly deduced and reflects the momentum loss caused by aerodynamic drag directly. The design trajectory points and corresponding weighting factors for the objective function are obtained reasonably. Constraints including; static margin, trim deflection angles, and hinge moment are imposed to ensure the static stability and controllability for the launch vehicle.

(4) Grid fins shape optimization problem of a launch vehicle is solved using the proposed SAO algorithm and CFD simulation. The objective function and constraints calculation tasks are accomplished automatically in batch mode using SolidWorks, ICEM CFD, and Fluent software's. The accuracy of the CFD method performed in this paper is tested using wind tunnel test data, and the calculated results of aerodynamic coefficients are in good agreement with the test results. The global optimal solution is obtained after 54 calling times of the original model, and 92 hours (3.84 days) computation time, which is highly favorable when compared to other evolutionary algorithms.

(5) The rockets shape possessing optimized grid fins satisfies all constraint conditions, and the weighted average drag coefficient as the objective function achieved is 11.07% less than the value of the baseline shape. By replacing the baseline shape with the optimized shape, it is observed that (a) taking the minimum fuel as an objective function, the take-off mass will be 2.07% lighter than the take-off mass of the baseline shape, (b) taking the maximum payload mass as an objective function, the payload mass will be 14.2% heavier than the payload mass of the baseline shape.

Acknowledgments

This work was supported by National University of Defense Technology Scientific Research Project [Grant No. ZK17-03-18] and Hunan Natural Science Foundation (Grant No. 2018JJ3591). The authors would like to thank Prof. Shifeng Zhang and Prof. Zhenyu Jiang for their valuable comments and suggestions in improving this paper.

References

Chen, S., Hong, X., Harris, C.J. Grey-box radial basis function modelling. Neurocomputing. 74, 1564-1571, 2011.

Deng, Y., Lam, I., Tor, S. A CAD-CAE integrated injection molding design system. Engineering Computations. 18, 80-92, 2002.

Erdem Dikbas, Özgür Uğraş Baran, Cuneyt Sert. Simplified Numerical Approach for the Prediction of Aerodynamic Forces on Grid Fins. Journal of Spacecraft and Rockets. 2018. (Online publication)

Gaetan K W Kenway, Joaquim R R A Martins. Multipoint aerodynamic shape optimization investigations of the common research model wing. AIAA Journal. 54, 113-128, 2016.

Gallard, F., Meaux, M., Montagnac, M. Aerodynamic aircraft design for mission performance by multipoint optimization. In: 21st AIAA Computational Fluid Dynamics Conference, San Diego, CA, 2013.

Goldberg, D. Genetic algorithms in search, optimization, and machine learning. New York: Addison-Wesley, 1989

Guyot, D., Schulein, E. Novel Locally Swept Lattice Wings for Missile Control at High Speeds. In: 45th AIAA Aerospace Sciences Meeting and Exhibit, Reno, Nevada, 2007.

Hardy, R.L. Multiquadratic equations of topography and other irregular surfaces. Journal of Geophysical Research. 76, 1905-1915, 1971.

Hastie, T., Tibshirani, R., Friedman, J. The elements of statistical learning. New York: Springer, 2001

Hu, F, Yang, X.-X, Jiang, Z.-Y, Zhang, W.-H. Integrated optimization design of trajectory/system parameters for solid launch vehicles. Journal of Solid Rocket Technology. 33. 599-602+610, 2010.

Hughson, M.C., Blades, E.L., Luke, E.A., Abate, G.L. Analysis of Lattice Grid Tailfin Missiles in High-Speed Flow. In: 25th AIAA Applied Aerodynamics Conference, Miami, FL, 2007.

Jae-Woo Lee,←Byung-Young Min, Yung-Hwan Byun. Multipoint Nose Shape Optimization of Space Launcher Using Response Surface Method. JOURNAL OF SPACECRAFT AND ROCKETS. 43, 137-147, 2006.

Jin, R., Chen, W., T, W.S. Comparative Studies of Metamodeling Techniques under Multiple Modeling Criteria. Journal of Structural and Multidisciplinary Optimization. 23, 1-13, 2001.

Jones, D.R. A taxonomy of global optimization methods based on response surfaces. Journal of Global Optimization. 21, 345-383, 2001.

Karaboga, D., Basturk, B. A powerful and efficient algorithm for numerical function optimization: artificial bee colony (ABC) algorithm. Journal of Global Optimization. 39, 459-471, 2003.

Kennedy, J., Eberhart, R. Particle swarm optimization. In: IEEE international conference on neural networks, Piscataway, 1995.

Kirkpatrick, S., Gelatt, C., Vecchi, M. Optimization by simulated annealing. Science. 220, 671-680, 1983.

Kitayama, S., Arakawa, M., Yamazaki, K. Sequential Approximate Optimization using Radial Basis Function network for engineering optimization. Optimization and Engineering. 12, 535-557, 2011.

Kitayama, S., Yamazaki, K. Simple estimate of the width in Gaussian kernel with adaptive scaling technique. Applied Soft Computing. 11, 4726-4737, 2011.

Kless, J.E., Aftosmis, M.J. Analysis of Grid Fins for Launch Abort Vehicle Using a Cartesian Euler Solver. In: 29th AIAA Applied Aerodynamics Conference, Honolulu, Hawaii, 2011.

Ledlow, T.W., Burkhalter, J.E., Hartfield, R.J. Integration of Grid Fins for the Optimal Design of Missile Systems. In: AIAA Atmospheric Flight Mechanics Conference, Kissimmee, Florida, 2015.

Lee, J., Min, B.Y., Byun, Y.H. Multipoint Nose Shape Optimization of Space Launcher Using Response Surface Method. Journal of Spacecraft and Rockets. 43, 137-146, 2006.

Luo, C., Zhang, S., Wang, C. A meta model-assisted evolutionary algorithm for expensive optimization. Journal of Computational and Applied Mathematics. 236, 759-764, 2011.

Luo, Y., Tang, G. Parallel Simulated Annealing Using Simplex Method. In: 10th AIAA/SSMO Multidisciplinary Analysis and Optimization Conference, New York, 2004.

Martijn H. A. Bonte, Lionel Fourment, Tien-tho Do, Optimization of forging processes using Finite Element simulations. Struct Multidisc Optim. 42, Struct Multidisc Optim, 2010.

Nakayama, H., Arakawa, M., Sasaki, R. Simulation-based optimization using computational intelligence. Optimization and Engineering. 3, 201-214, 2002.

Padula, S.L., Alexandrov, N., Green, L.L. MDO Test Suite at NASA Langley Research Center. In: 6th AIAA/NASA/ISSMO symposium on multidisciplinary analysis and optimization, Bellevue, WA, 1996.

Parzen, E. On estimation of a probability density function and mode. Annals of Mathematical Statistics. 33, 1065-1076, 1962.

Peng, K., Hu, F., Zhang, W., Zhou, Z. Review of grid fin aerodynamic characteristics and application. Journal of Solid Rocket Technology. 38, 458-464 (In Chinese), 2015.

Simpson, M.G., Sadler, J.A. Controls: a Comparison with Conventional Planar Fins. In: RTO AVT Symposium, Sorrento, Italy, 1998.

Sunago, M., Sasaki, D., Takenaka, K., Nakahashi, K. Multipoint Optimization of a Short-Range Quiet Passenger Aircraft. Journal of Aircraft. 46, 1070-1074, 2009.

Theerthamalai P, Nagarathinam M. Aerodynamic Analysis of Grid-Fin Configurations at Supersonic Speeds. JOURNAL OF SPACECRAFT AND ROCKETS. 43, 750-756, 2006.

Theerthamalai, P. Aerodynamic Characterization of Grid Fins at Subsonic Speeds. Journal of Aircraft. 44, 694-697, 2007.

Wang, D., Wu, Z., Fei, Y., Zhang, W. Structural design employing a sequential approximation optimization approach. Computers and Structures. 134, 75-87, 2014.

Wang, D., Hu, F., Ma, Z., Wu, Z., Zhang, W. A CAD/CAE integrated framework for structural design optimization using sequential approximation optimization. Advances in Engineering Software. 76, 56-68, 2014.

Washington, D.W., Miller, M.S. Experimental investigations of grid fin aerodynamics: a synopsis of nine wind tunnel and three

flight tests. In: Proceedings of RTO AVT Symposium on Missile Aerodynamic, Sorrento, Italy, 1998.

Washington, W.D., Booth, P.F., Miller, M.S. Curvature and Leading Edge Sweep Back Effects on Grid Fin Aerodynamic Characteristics. In: 11th Applied Aerodynamics Conference, Monterey, CA, 1993.

Wu, Zeping, Wang, Donghui, Okolo, Patrick, Jiang, Zhenyu, Zhang, Weihua. Unified estimate of Gaussian kernel width for surrogate models. Neurocomputing. 203, 41–51, 2016.

Wu, Zeping, Donghui, Wang, Weihua, Zhang, Okolo, Patrick, Yang, Fei. Solid-rocket-motor performance matching design framework. J Spacecraft Rockets. 54, 1–10, 2017.

Xiao CHAI, Xiongqing YU, Yu WANG. Multipoint optimization on fuel efficiency in conceptual design of wide-body aircraft. Chinese Journal of Aeronautics. 31, 99-106, 2018.

Xiong, Y., Chen, W., Apley, D., Ding, X. A non-stationary covariance-based Kriging method for meta-modeling in engineering design. International Journal for Numerical Methods in Engineering. 71, 733-756, 2007.

Xu, P., Jayawardena, A.W., Li, W.K. Model selection for RBF network via generalized degree of freedom. Neurocomputing. 99, 163-171, 2013.

Yang, X., Zhang, W. A faster optimization method based on support vector regression for aerodynamic problems. Advances in Space Research. 52, 1008-1017, 2013.

Yeh, I., Chen, C., Zhang, X., Wu, C., Huang, K. Adaptive radial basis function networks with kernel shape parameters. Neural Computing and Applications. 21, 469-480, 2012.

Yildiz, A. An effective hybrid immune-hill climbing optimization approach for solving design and manufacturing optimization problems in industry. Journal of Materials Processing Technology. 209, 2773-2780, 2009.